
International Journal of Electronics
Publication details, including instructions for authors and subscription information:
http://www.tandfonline.com/loi/tetn20

# Sliding mode control and stability analysis of buck DC-DC converter

J.-F. Tsai [a] & Y.-P. Chen [a]
[a] Department of Electrical and Control Engineering , National Chiao Tung University , 1001 Ta Hsueh Road, Hsinchu, 300, ROC
Published online: 26 Feb 2007.

To cite this article: J.-F. Tsai & Y.-P. Chen (2007) Sliding mode control and stability analysis of buck DC-DC converter, International Journal of Electronics, 94:3, 209-222, DOI: 10.1080/00207210601176692

To link to this article: http://dx.doi.org/10.1080/00207210601176692

*International Journal of Electronics*,
Vol. 94, No. 3, March 2007, 209–222

Taylor & Francis
Taylor & Francis Group

# Sliding mode control and stability analysis of buck DC-DC converter

J.-F. TSAI* and Y.-P. CHEN

Department of Electrical and Control Engineering,
National Chiao Tung University, 1001 Ta Hsueh Road, Hsinchu, 300, ROC

(*Received 26 September 2004; in final form 14 January 2007*)



This paper is proposed to deal with the voltage regulation of buck DC-DC converter based on sliding mode control (SMC) technology. A buck DC-DC converter with parasitic resistance is inherently a bilinear system possessing inevitable uncertainties, such as variable resistive load and input disturbance. First, the buck DC-DC converter is modified into an uncertain linear model. Then, SMC technology is adopted to suppress the input disturbance and reduce the effects from the load variation. In addition, the continuous conduction mode (CCM) for normal operation can be guaranteed by the design of sliding function. Finally, experimental results are included for demonstration.

*Keywords*: Buck DC-DC converter; Reaching and sliding region (RAS-region); Sliding mode control (SMC); Voltage regulation

## 1. Introduction

With the switching property, the sliding mode theory provides an intuitive way to control switching converters (Sira-Ramirez 1987, Sira-Ramirez and Ilic 1988). Compared to the state space average method (Mohan *et al*. 1995), the sliding mode theory leads to large signal stability. Besides, it is robust to uncertainties and much easier in implementation. Up to now, several control strategies for switching converters based on sliding mode theory have been proposed (Sira-Ramirez 1987, Sira-Ramirez and Ilic 1988, Carpita and Marchesoni 1996, Caceres and Barbi 1999, Escobar *et al*. 1999). Sira-Ramirez (1987) presented detailed analysis of bilinear switched networks and showed that the buck DC-DC converter could keep on the sliding regimes and achieve the constant regulation with indirect control for an exact system model. In addition, Carpita and Marchesoni (1996) successfully presented a robust SMC for a buck DC-DC converter with resistive-load variation and input disturbance; however, they did not consider how the system performance is affected by the choice of sliding function.

For simplicity, a buck DC-DC converter is conventionally modelled as a linear system by neglecting the unknown parasitic resistance, which usually results in a small uncertain deviation and then reduces the system precision. For improvement, the unknown parasitic resistance should be taken into consideration, which means

*Corresponding author. Email: u9012803@cc.nctu.edu.tw

*International Journal of Electronics*
ISSN 0020–7217 print/ISSN 1362–3060 online © 2007 Taylor & Francis
http://www.tandf.co.uk/journals
DOI: 10.1080/00207210601176692

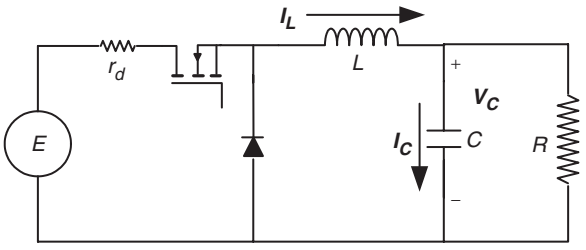


Figure 1. Buck DC-DC converter with resistive load.



the buck DC-DC converter is modelled as an uncertain bilinear system. However, it is not easy work to deal with such an uncertain bilinear model via control technologies. In this paper, the uncertain bilinear model is first changed into a linear form through suitable state variables transformation, and then the sliding mode control algorithm is employed for the buck DC-DC converter design.

In general, most of the researches base on the assumption that the buck DC-DC converter operates only in the continuous conduction mode (CCM). However, if the circuit components' values are not appropriately selected, the buck DC-DC converter may operate in the discontinuous conduction mode (DCM). In this paper, with the sliding mode control algorithm, the buck DC-DC converter is finally driven to the sliding line and then stays on it, regardless of the existence of DCM during the transient.

The remainder of this paper is organized as follows. In § 2, the model of a buck DC-DC converter with parasitic resistance is first introduced as an uncertain bilinear form, and then modified into an uncertain linear model. Section 3 shows the design procedure of sliding mode control and the system stability analysis. Section 4 gives experimental results subject to load variation, input disturbance and the effects caused by different choices of sliding functions. Finally, conclusions are given in § 5.

## 2. Model description

The buck DC-DC converter with resistive load $R$ is illustrated in figure 1, where $E$ is the DC voltage source, $L$ is the inductance, $C$ is the capacitance, and $r_d$ is the parasitic resistance. Note that $R = R_0 + \Delta R$, where $R_0$ is the nominal resistive load and $\Delta R$ varies in the range of $[\delta r_1, \delta r_2]$. Clearly, $R \in [R_{\min}, R_{\max}]$, where $R_{\min} = R_0 + \delta r_1$ and $R_{\max} = R_0 + \delta r_2$.

Assume the buck DC-DC converter is operating in continuous conduction mode (CCM), then, the state equation can be expressed as

$$\begin{bmatrix} \dot{I}_L \\ \dot{V}_C \end{bmatrix} = \begin{bmatrix} 0 & -\dfrac{1}{L} \\ \dfrac{1}{C} & -\dfrac{1}{RC} \end{bmatrix} \begin{bmatrix} I_L \\ V_C \end{bmatrix} + \begin{bmatrix} -\dfrac{r_d}{L} & 0 \\ 0 & 0 \end{bmatrix} \begin{bmatrix} I_L \\ V_C \end{bmatrix} u + \begin{bmatrix} \dfrac{E}{L} \\ 0 \end{bmatrix} u \tag{1}$$

where $V_C$ is the capacitor voltage, $I_L$ is the inductor current, and $u$ represents the switching input with value 0 or 1. Note that (1) is linear in control and linear in state

variables $V_C$ and $I_L$, but not jointly linear in control and state variables. That means it is a bilinear system (Mohler 1991).

Let the desired output capacitor voltage be a constant $V_{Cd}$. Define $V_C - V_{Cd}$ and $I_C/C$ as the new state variables, $x_1$ and $x_2$, then

$$\dot{x}_1 = \frac{d(V_C - V_{Cd})}{dt} = \frac{dV_C}{dt} = \frac{I_C}{C} = x_2 \tag{2}$$

From figure 1, it is easy to obtain that

$$I_L = I_C + \frac{V_C}{R} = Cx_2 + \frac{x_1 + V_{Cd}}{R} \tag{3}$$

Further differentiating (3) and using the first equation in (1), it leads to

$$\dot{x}_2 = -\frac{1}{CL}x_1 - \frac{1}{CR}x_2 + \frac{E}{CL}u - \frac{r_d}{CL}I_L u - \frac{V_{Cd}}{CL} \tag{4}$$

Let $\mathbf{x} = [x_1 x_2]^T$, then (2) and (3) could be rewritten as

$$\dot{\mathbf{x}} = \mathbf{A}\mathbf{x} + (\mathbf{B} + \Delta\mathbf{B}(\mathbf{x}))u + \mathbf{h} \tag{5}$$

where

$$\mathbf{A} = \begin{bmatrix} 0 & 1 \\ -\dfrac{1}{CL} & -\dfrac{1}{CR} \end{bmatrix} \tag{6}$$

$$\mathbf{B} = \begin{bmatrix} 0 \\ \dfrac{E}{CL} \end{bmatrix} \tag{7}$$

$$\Delta\mathbf{B}(\mathbf{x}) = \begin{bmatrix} 0 \\ -\dfrac{r_d}{CL}I_L \end{bmatrix} = \begin{bmatrix} 0 \\ -\dfrac{r_d}{CLR}x_1 - \dfrac{r_d}{C}x_2 - \dfrac{r_d V_{Cd}}{CLR} \end{bmatrix} \tag{8}$$

$$\mathbf{h} = \begin{bmatrix} 0 \\ -\dfrac{V_{Cd}}{CL} \end{bmatrix} \tag{9}$$

Significantly, the bilinear system (1) is changed into (5), which is a linear system with control input $u$ and encounters the state-dependent uncertainty $\Delta\mathbf{B}(\mathbf{x})$ and external input $\mathbf{h}$. Obviously, both $\Delta\mathbf{B}(\mathbf{x})u$ and $\mathbf{h}$ are matched disturbances and thus it is suitable to design the controller by using the sliding mode technique.

## 3. Sliding mode controller design and phase plane analysis

### 3.1 *Design procedure of sliding mode controller*

In general, there are two fundamental steps to design a sliding mode control. First, choose an appropriate sliding function $s$ to guarantee the system stability in the sliding mode $s = 0$. Second, derive the control algorithm such that the system trajectory reaches the sliding surface in a finite time and then stays thereafter.

However, unlike the conventional sliding mode control input, the control $u$ in (5) only switches between 0 and 1, which makes the controller design more restrictive.

In the first step, the sliding function is chosen as

$$s = x_2 + \lambda x_1 \tag{10}$$

where $\lambda(\lambda > 0)$ is a constant. It guarantees the system in the sliding mode $s = 0$ is stable, i.e., $x_1(t) \to 0$ as $t \to \infty$. For the second step, the control algorithm is purposely designed as

$$u = 0.5(1 - \text{sign}(s)) \tag{11}$$

which obviously switches between 0 and 1 depending on the scalar sign of $s$. Most importantly, (11) must satisfy the following reaching and sliding condition

$$s\dot{s} < 0, \quad \forall\, s \neq 0 \tag{12}$$

such that the system trajectories could reach the sliding line in a finite time and then stay thereafter (Slotine and Li 1991, Utkin 1978). From (5) and (10), the derivative of the sliding function with respect to time is

$$\dot{s} = -\frac{1}{CL}x_1 + \left(\lambda - \frac{1}{CR}\right)x_2 + \frac{E}{CL}u - \frac{r_d}{CL}I_L u - \frac{V_{Cd}}{CL} \tag{13}$$

Further substituting the control algorithm $u$ in (11) leads to

$$\dot{s} = \begin{cases} -\dfrac{1}{CL}x_1 + \left(\lambda - \dfrac{1}{CR}\right)x_2 + \dfrac{E - r_d I_L}{CL} - \dfrac{V_{Cd}}{CL} & \text{for } s < 0 \\ -\dfrac{1}{CL}x_1 + \left(\lambda - \dfrac{1}{CR}\right)x_2 - \dfrac{V_{Cd}}{CL} & \text{for } s > 0 \end{cases} \tag{14}$$

Clearly, if

$$\frac{V_{Cd}}{CL} - \frac{E - r_d I_L}{CL} < -\frac{1}{CL}x_1 + \left(\lambda - \frac{1}{CR}\right)x_2 < \frac{V_{Cd}}{CL} \tag{15}$$

then the reaching and sliding condition (12) is guaranteed. The region described in (15) is defined as the reaching and sliding region or RAS-region (Chen *et al.* 2000) in brief. By replacing $I_L$ given in (3), the inequality (15) can be rewritten into

$$\begin{aligned} \frac{(R + r_d)V_{Cd} - ER}{RCL} < &-\frac{(R + r_d)}{RCL}x_1 + \left(\lambda - \frac{1}{RC} - \frac{r_d}{L}\right)x_2 \\ &-\frac{1}{CL}x_1 + \left(\lambda - \frac{1}{RC}\right)x_2 < \frac{V_{Cd}}{CL} \end{aligned} \tag{16}$$

Clearly, the RAS-region is bounded by two lines, $\sigma_1$ and $\sigma_2$, with slopes $m_1 = (R + r_d)/(LRC\lambda - L - RCr_d)$ and $m_2 = R/(LRC\lambda - L)$ respectively, which are related to the unknown parasitic resistance $r_d$ and the value of $\lambda$ chosen for sliding function $s$ in (10). The relationship between the slopes of $\sigma_1$, $\sigma_2$ and sliding line are classified into six cases given in table 1 and shown in figure 2. Note that $\mathbf{P}_1((RV_{Cd} + r_d V_{Cd} - ER)/(R + r_d), 0)$ and $\mathbf{P}_2(-V_{Cd}, 0)$ are the points of $\sigma_1$ and $\sigma_2$ crossing $x_1$-axis.

Table 1. The relationship between the slopes of $\sigma_1$, $\sigma_2$ and sliding line.

| Case | $\lambda$ | $m_1$ $m_2$ |
|---|---|---|
| A | $0<\lambda\leq 1/RC-R/L$ | $m_1<0$, $m_2<0$, $m_2\leq m_1<-\lambda$ $(L/C>R^2)$ |
| B | $1/RC-R/L<\lambda<1/RC$ | $m_1<0$, $m_2<0$, $m_2<m_1<-\lambda$ |
| C | $\lambda=1/RC$ | $m_1<0$, $m_2=\infty$, $m_1<-\lambda<m_2$ |
| D | $1/RC<\lambda<1/RC+r_d/L$ | $m_1<0$, $m_2>0$, $m_1<-\lambda<m_2$ |
| E | $\lambda=1/RC+r_d/L$ | $m_1=\infty$, $m_2>0$, $-\lambda<m_2<m_1$ |
| F | $1/RC+r_d/L<\lambda$ | $m_1>0$, $m_2>0$, $-\lambda<m_2<m_1$ |

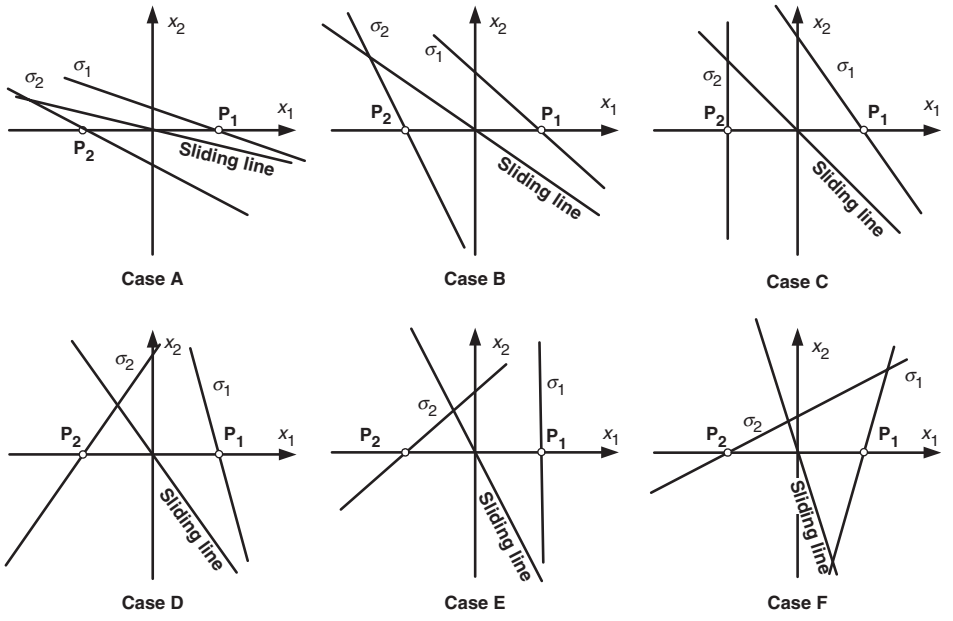


Figure 2. Six cases of the relationship between the $\sigma_1$, $\sigma_2$ and sliding line in the phase plane.

### 3.2 *Phase plane analysis*

In normal operation, the output voltage $V_C$ of the buck DC-DC converter is non-negative, which implies

$$x_1 = V_C - V_{Cd} \geq -V_{Cd} \tag{17}$$

and then the system trajectory should be inherently in the right-half plane $x_1 \geq -V_{Cd}$. Moreover, when the buck DC-DC converter operates in the CCM, described by (3), the inductor current $I_L$ should be greater than zero and thus

$$I_C(t) > -\frac{V_C(t)}{R} \tag{18}$$

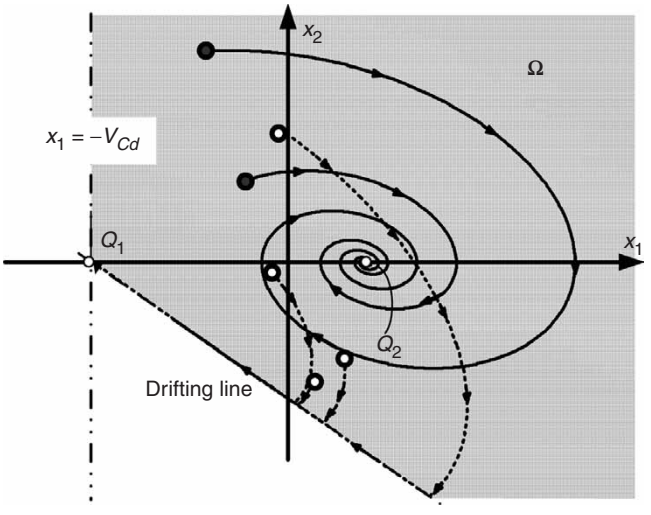


Figure 3. System trajectories with different initial conditions.

If the components of the buck DC-DC converter are not carefully designed, it may fall into the DCM with $I_L = 0$, governed as

$$I_C(t) = -\frac{V_C(t)}{R} \tag{19}$$

Since $x_1 = V_C - V_{Cd}$ and $x_2 = I_C/C$, (18) and (19) can be rewritten as

$$x_1 + RCx_2 > -V_{Cd} \tag{20}$$

and

$$x_1 + RCx_2 = -V_{Cd} \tag{21}$$

which is named as the drifting line in this paper and represents the DCM. According to (17), (20) and (21), the system trajectory of a buck DC-DC converter should be restricted to the following region

$$\Omega = \begin{cases} x_1 \geq -V_{Cd} \\ x_1 + RCx_2 \geq -V_{Cd} \end{cases} \tag{22}$$

as shown in figure 3, where the system trajectories with different initial conditions are also included for $u = 0$ (dashed-lines) and $u = 1$ (solid-lines), which will converge to $Q_1(-V_{Cd}, 0)$ and $Q_2(E - V_{Cd}, 0)$, respectively. Later, dashed-lines and solid-lines will denote the trajectories of $u = 0$ and $u = 1$, respectively in the phase plane. All the trajectories with $u = 0$ are moving clockwise to reach the drifting line first and then approach to $Q_1$. As regards the trajectories with $u = 1$, they are moving spirally clockwise to $Q_2$.

According to table 1, the RAS-regions (12) could be mainly classified into two types: $\lambda \leq 1/RC$ as Type-I and $\lambda > 1/RC$ as Type-II. Clearly, Type-I consists of cases A, B and C and Type-II consists of cases D, E and F. For Type-I, $\Omega$ is the

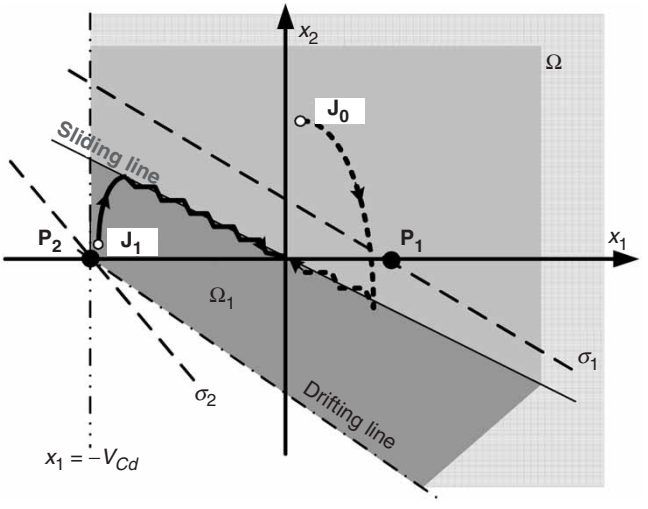


Figure 4. System trajectories for the cases of Type-I.

RAS-region and separated into $\Omega_0$ and $\Omega_1$ by $s=0$ as depicted in figure 4. From (16), $\Omega_0$ and $\Omega_1$ are bounded as

$$\Omega_0 = \begin{cases} s>0 \\ \sigma_2<0 \\ x_1> -V_{Cd} \\ x_1 + RCx_2> -V_{Cd} \end{cases} \quad \text{for } u=0 \tag{23}$$

$$\Omega_1 = \begin{cases} s<0 \\ \sigma_1>0 \\ x_1> -V_{Cd} \\ x_1 + RCx_2> -V_{Cd} \end{cases} \quad \text{for } u=1 \tag{24}$$

Two system trajectories related to $J_0$ in $\Omega_0$ and $J_1$ in $\Omega_1$ are also shown in figure 4, where $J_0$ and $J_1$ represent the initial conditions. Since all the trajectories in $\Omega_0$ and $\Omega_1$ satisfy the reaching condition (12), the trajectories starting from $J_0$ and $J_1$ will approach the sliding line in a finite time and then maintain there to generate the desired sliding mode $s=0$. From (10), the system behaviour is exponentially stable in the sliding mode. Obviously, with the sliding mode controller (11), the reaching and sliding condition is globally satisfied for cases of Type-I. Moreover, it could be seen that none of the system portraits will enter the drifting line. Thus, if the following inequality is satisfied

$$\lambda < \frac{1}{R_{\max} C} \tag{25}$$

then the buck DC-DC converter will operate only in CCM, which is achieved by (25) rather than the assumption as given in Sira-Ramirez (1987), Sira-Ramirez and Ilic (1988) and Carpita and Marchesoni (1996).

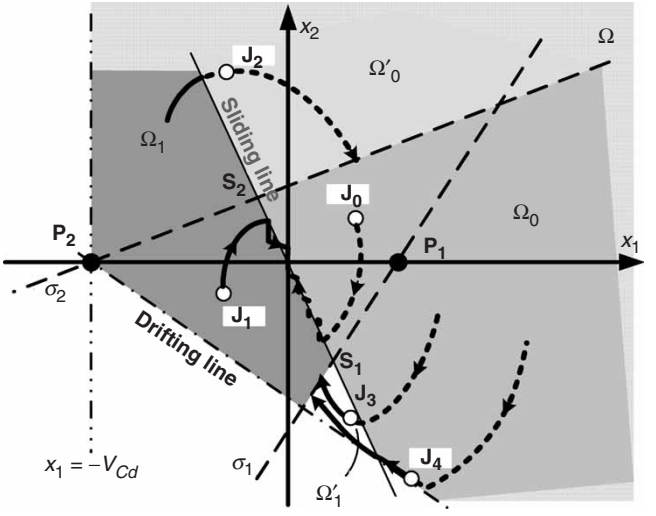


Figure 5. System trajectories for the cases of Type-II.

As for the cases of Type-II, the system behaviour is more complicated than Type-I, due to the reaching and sliding condition, being only locally satisfied. Also, from (16), four sub-regions, $\Omega_0$, $\Omega'_0$, $\Omega_1$ and $\Omega'_1$, shown in figure 5, are bounded as

$$\Omega_0 = \begin{cases} s > 0 \\ \sigma_2 < 0 \\ x_1 > -V_{Cd} \\ x_1 + RCx_2 > -V_{Cd} \end{cases} \quad \text{for } u = 0 \tag{26}$$

$$\Omega'_0 = \begin{cases} s > 0 \\ \sigma_2 > 0 \end{cases} \quad \text{for } u = 0 \tag{27}$$

$$\Omega_1 = \begin{cases} s < 0 \\ \sigma_1 > 0 \\ x_1 > -V_{Cd} \\ x_1 + RCx_2 > -V_{Cd} \end{cases} \quad \text{for } u = 1 \tag{28}$$

$$\Omega'_1 = \begin{cases} s < 0 \\ \sigma_1 < 0 \\ x_1 + RCx_2 > -V_{Cd} \end{cases} \quad \text{for } u = 1 \tag{29}$$

where $\Omega_0$ and $\Omega'_0$ are related to $u = 0$ and $\Omega_1$ and $\Omega'_1$ are related to $u = 1$.

There are mainly five kinds of trajectories shown in figure 5 corresponding to different points $J_0$, $J_1$, $J_2$, $J_3$ and $J_4$ to reach the sliding line. For the trajectories about $J_0$ and $J_1$, they are just like the cases of Type-I, which will reach the sliding line in a finite time. For the trajectory about $J_2$, it may come from $\Omega_1$ or start from $\Omega'_0$.

From figure 5, the trajectory must get into the sub-region $\Omega_0$. For the trajectory about $J_3$, it may come from $\Omega_0$ or starts from $\Omega_1'$. Also, viewing from figure 5, the trajectory has to enter the sub-region $\Omega_1$. Finally, for the trajectory about $J_4$, it comes from $\Omega_0'$ and then along the drifting line for $u=0$. Once the trajectory passes through the sliding line, it will get into the sub-region $\Omega_1'$ where the control input is changed to be $u=1$. According to trend of these five trajectories, they all will be forced to reach the segment between $\mathbf{S}_1$ and $\mathbf{S}_2$ of the sliding line and then move along it to the origin. Unlike the cases of Type-I, system portraits of Type-II may consist of both CCM and DCM during the transient, but they can be still successfully driven into the sliding line and kept on $s=0$ with a larger convergent rate comparing to those of Type-I.

From the above analysis, it is clear that the sliding mode controller (11) could drive the system, Type-I and Type-II, to reach the sliding line and then converge to the origin.



### 3.3 *Robustness analysis*

From (5), if varying resistive load leads to matched disturbances, it could be written as

$$\dot{\mathbf{x}} = (\mathbf{A}_0 + \delta\mathbf{A})\mathbf{x} + \mathbf{B}u + \Delta\mathbf{B}(\mathbf{x})u + \mathbf{h} \tag{30}$$

where

$$\mathbf{A}_0 = \begin{bmatrix} 0 & 0 \\ -\dfrac{1}{CL} & -\dfrac{1}{CR_0} \end{bmatrix} \tag{31}$$

are related to the nominal parts of the system. Besides, $\delta\mathbf{A}\mathbf{x}$, $\Delta\mathbf{B}(\mathbf{x})u$ and $\mathbf{h}$ are all treated as matched disturbances since

$$\delta\mathbf{A}\mathbf{x} = \mathbf{B}\left(-\frac{\Delta RCL}{CR_0(R_0+\Delta R)E}x_2\right) = \mathbf{B}d_{\mathbf{A}} \tag{32}$$

$$\Delta\mathbf{B}(\mathbf{x})u = \mathbf{B}\left(-\frac{r_d}{(R_0+\Delta R)E}x_1 - \frac{r_d L}{E}x_2 - \frac{r_d V_{Cd}}{(R_0+\Delta R)E}\right)u = \mathbf{B}d_{\mathbf{B}} \tag{33}$$

$$\mathbf{h} = \mathbf{B}\left(\frac{-V_{Cd}}{E}\right) = \mathbf{B}d_{\mathbf{h}} \tag{34}$$

Hence, (30) can be rearranged as

$$\dot{\mathbf{x}} = \mathbf{A}_0\mathbf{x} + \mathbf{B}u + \mathbf{B}(d_{\mathbf{A}} + d_{\mathbf{B}} + d_{\mathbf{h}}) \tag{35}$$

According to the sliding mode theory, all the matched disturbances $\mathbf{B}d_{\mathbf{A}}$, $\mathbf{B}d_{\mathbf{B}}$ and $\mathbf{B}d_{\mathbf{h}}$ will be eliminated once the system trajectory is restricted on sliding line. Thus, the system behaviour is insensitive to load variation $\Delta R$, which will be demonstrated in experiment later.

Table 2. Parameters of the buck DC-DC converter.

| Parameter | $E$ | $L$ | $C$ | $L_r$ | $R_0$ | $V_{Cd}$ |
|---|---|---|---|---|---|---|
| Value | 12.28(V) | 2.47(mH) | 470(μF) | 0.7(Ω) | 15.35(Ω) | 8(V) |

## 4. Experimental results

A lab-prototype of buck DC-DC converter for theoretically verifying is fabricated, which consists of a current sensor LTS-6NP and a PC-based controller with NI-6024E. The maximum sampling rate is limited to 20 KHz and the parameters of the circuit are listed in table 2. Next, three examples are given to show the effect caused by different sliding functions and load variation.

**Example 1:** The experimental results in figure 6(a)–(c) are obtained for different sliding functions with $\lambda = 100$, $\lambda = 500$ and $\lambda = 1000$. Figure 6(a) shows the system trajectories in the phase plane. Clearly, all the trajectories are successfully driven to the sliding lines and then approach to the origin. Note that the case of $\lambda = 100$ is corresponding to the trajectory of Type-I in figure 4 passing or starting from $J_1$. As to the cases of $\lambda = 500$ and 1000, their trajectories are of Type-II in figure 5 passing or starting from $J_1$. From figure 6(b), it is easy to find that the system trajectories will reach the sliding modes faster for smaller λ. However, it can also be seen from figure 6(c) that smaller λ results in slow convergent rate for the output voltage to the desired value. Moreover, from figure 6(c), the steady state errors are resulted from the inevitable measuring noise and they can be reduced when λ is increased. In this example, it can be concluded that with larger λ, the SMC can provide faster dynamics and tolerate larger measuring noise.

**Example 2:** Let $\lambda = 100$, 3500 and 20000. The experimental results shown in figure 7(a)–(c) actually confirm the predicted dynamics in § 3. Figure 7(a) shows the system trajectories corresponding to $J_1$ for Type-I in figure 4 and corresponding to $J_2$ and $J_4$ for Type-II in figure 5 with $\lambda = 100$, 3500 and 20000, respectively. Note that the trajectory for the case of $\lambda = 20000$ contains DCM during the transient. From figure 7(b), it can be found that two of sliding functions for $\lambda = 3500$ and $\lambda = 20000$ do not always converge; however, they will finally converge to zero after a short time. Unlike example 1, figure 7(c) shows that larger λ results in larger overshoot, which may be undesirable in some applications.

This example shows that the system performance will be converged faster for larger λ. Besides, larger λ may also result in larger overshoot or drive the buck converter into DCM during the transient. More significantly, from figure 7(a)–(c), the SMC successfully drives the buck DC-DC converter into the sliding line and, finally, achieves the desired performance.

**Example 3:** Let $\lambda = 1000$, 3300, 4000 and 20000, respectively and the buck converter is connected to two distinct resistive load as $R = 20.5\,\Omega$ and $R = 6.9\,\Omega$. Figure 8 shows the experimental results of the output voltage error where $\psi_1$ and $\psi_2$ symbol for the cases of $R = 20.5\,\Omega$ and $R = 6.9\,\Omega$, respectively. It is shown that the system is robust to load variation. Moreover, it is obvious that with the same λ,

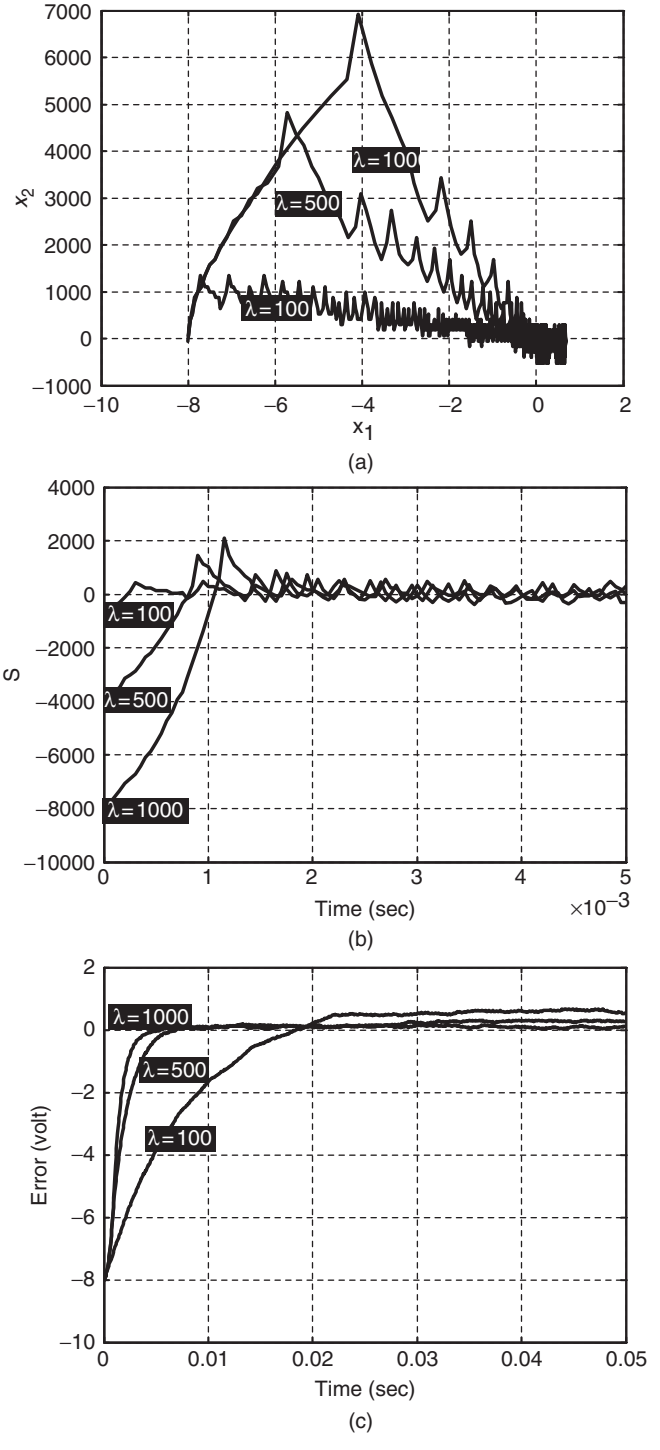


Figure 6. (a) The system trajectories in the phase plane with different λ; (b) sliding functions with different λ; (c) errors of the output voltage with different sliding function.

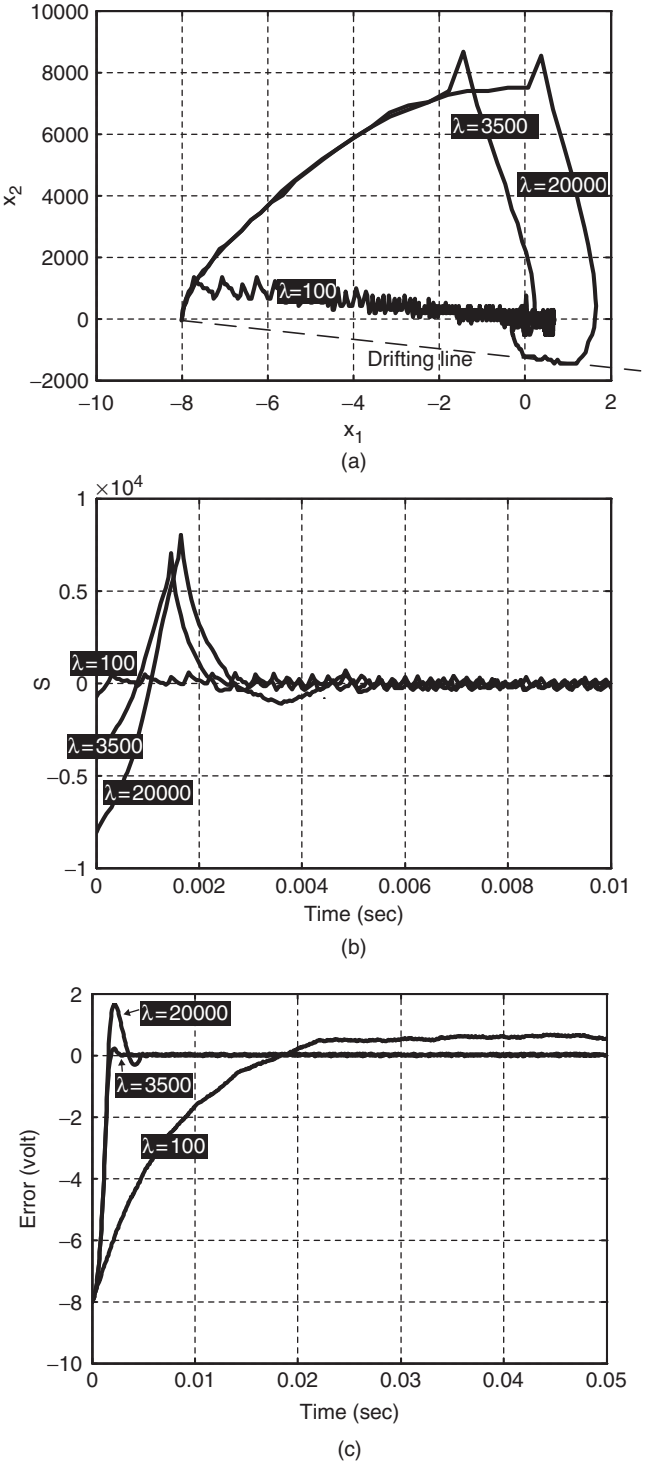


Figure 7. (a) The system trajectories in the phase plane with different λ; (b) the sliding function with different λ; (c) errors of the output voltage with different λ.

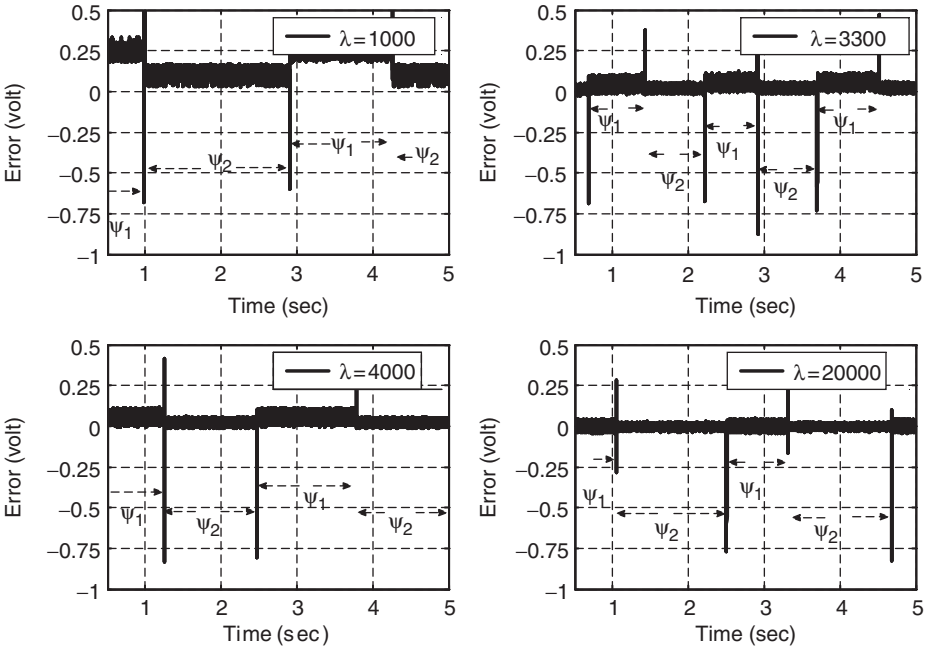


Figure 8. Errors of the output voltage with unexpected load variation.

Table 3. Tune-up of λ in terms of the desired performance.

| Desired performance | λ |
|---|---|
| Reduce overshoot | Decreased |
| Reduce output error | Increased |
| Increase convergent rate | Increased |

the error is reduced when the load $R$ is changed from 20.5 Ω to 6.9Ω. It is because the signal-to-noise ratio is higher for smaller resistive load.

From above examples, one can assign a suitable λ to attain a desired performance, which is listed in table 3. If the overshoot is larger than the desired specification, it can be improved by decreasing the value of λ according to figure 7(c). If the output error is larger than the acceptable value, it can be reduced by increasing λ according to figure 6(c). While the convergent rate is too slow, it can be accelerated by increasing λ also viewing from figure 6(c).

## 5. Conclusion

An alternative model of buck DC-DC converter with uncertain bilinear terms is introduced in this paper. With the proposed SMC, the buck DC-DC converter is robust to resistive load variation. The RAS-region is analysed in detail with respect to different sliding functions. Significant system behaviours for Type-I and Type-II

are also depicted completely in phase plane. Finally, experimental results are given to verify the predicted system performances of the buck DC-DC converter by using the SMC in this paper.

**Acknowledgement**

The work of this paper was supported by a grant provided by Ministry of Education, Taiwan, ROC(EX-91-E-FA06-4-4).



**References**

R.O. Caceres and I. Barbi, "A boost DC-AC converter: analysis, design, and experimentation", *IEEE Trans. on Power Elect*., 14, pp. 134–141, 1999.

M. Carpita and M. Marchesoni, "Experimental study of a power conditioning system using sliding mode control", *IEEE Trans. on Power Elect*., 11, pp. 731–742, 1996.

Y.P. Chen, J.L. Chang and K.M. Lai, "Stability analysis and bang-bang sliding control of a class of single-input bilinear systems", *IEEE Trans. on Autom. Cont*., 45, pp. 2150–2154, 2000.

G. Escobar, R. Ortega, H. Sira-Ramirez, J.P. Vilain and I. Zein, "An experimental comparison of several nonlinear controllers for power converters", *IEEE Cont. Syst. Magazine*, 19, pp. 66–82, 1999.

N. Mohan, T.M. Undeland and W.P. Robbins, *Power Electronics: Converters, Applications, and Design*, 2nd edn, New York: John Wiley & Sons, 1995.

R.R. Mohler, *Nonlinear Systems*, Volume II, *Applications to Bilinear Control*, Englewood Cliffs, NJ: Prentice-Hall, 1991.

H. Sira-Ramirez, "Sliding motions in bilinear switched networks", *IEEE Trans. on Circuits Syst*., CAS-34, pp. 919–933, 1987.

H. Sira-Ramirez and M. Ilic, "A geometric approach to the feedback control of switch mode dc-to-dc power supplies", *IEEE Trans. on Circuits Syst*., 35, pp. 1291–1298, 1988.

J.-J.E. Slotine and W. Li, *Applied Nonlinear Control*, New York: Prentice-Hall, 1991.

V.I. Utkin, *Sliding Regimes and Their Applications in Variable Structure Systems*, Moscow: MIR, 1978.